

# Electronic structures of spinel nickel cobaltite from a spin-polarized quasi-particle self-consistent GW method

メタデータ	言語: eng 出版者: 公開日: 2021-03-17 キーワード (Ja): キーワード (En): 作成者: メールアドレス: 所属:
URL	<a href="http://hdl.handle.net/2297/00061344">http://hdl.handle.net/2297/00061344</a>

This work is licensed under a Creative Commons Attribution-NonCommercial-ShareAlike 3.0 International License.



## Abstract

Electronic structures of spinel nickel cobaltite from a spin-polarized quasi-particle self-consistent  
GW method

スピン分極準粒子自己無撞着 GW 法による  
スピネル-ニッケル-コバルタイトの電子構造

Graduate School of  
Natural Science & Technology  
Kanazawa University

Division of Mathematical and Physical Sciences

Student ID No. 1724012006  
Name: Hasan Al Rasyid  
Chief Advisor: Professor Tatsuki ODA  
Date of Submission: July 2, 2020

## ABSTRACT

Quasi-particle self-consistent GW (QSGW) electronic structure calculation was performed in three spinel structures of  $\text{NiCo}_2\text{O}_4$ , i.e. normal spinel and two of inverse spinel structures (Types A and B). The results were compared with those from the density functional theory (DFT) based on generalized gradient approximation (GGA). In this dissertation, we also compare  $\text{NiCo}_2\text{O}_4$  with other material that have similar structure, namely  $\text{NiCo}_2\text{S}_4$  and  $\text{Co}_3\text{O}_4$ . Half-metallicity was observed in the all cases investigated, where the band energy gap appears in the majority spin state. The QSGW indicated that the gap is larger than that of the corresponding GGA case. The QSGW may yield more localized  $d$ -orbitals, compared with those from the GGA. In basis of projected density of states (PDOS) analysis, Co atoms of octahedral site [Co(oct)] were found to be a non-magnetic/weak magnetic configuration (low spin state) among them, resulting in a negligible contribution to the total magnetization. The largest contribution to the total magnetization is provided by Co atoms of tetrahedral [Co(tet)] site (high spin state). In the QSGW calculation, the electronic states near the Fermi level consists mainly of Co(tet) 3d  $e_g$ -orbitals. In the normal and inverse (type A) spinels, the Fermi level cross the states with the DOS having a large sharp peak, implying instability of electronic structure. The results of QSGW were discussed by comparing with those of one-shot GW and other methods. Comparing  $\text{NiCo}_2\text{O}_4$  and  $\text{NiCo}_2\text{S}_4$ , we found that metallic behaviour mainly come from hybridization between 3d orbital of Co(Td) with p orbital of oxygen or sulfide. We also found that sulfide anion provides more localized electron than Oxygen anion. The introduction of Ni induces  $\text{NiCo}_2\text{O}_4$  to be metallic. However, at the end, Ni would have minimal contribution to the single-spin state conductivity (half-metal). This raise a speculation on crucial role of Ni(Td) in dictating metallicity of  $\text{NiCo}_2\text{O}_4$ .

## 1 INTRODUCTION

### 1.1 Research background and Motivation

Oxygen reduction reaction (ORR) is one of the most basic reactions that construct many complex reactions such as energy generation (fuel cell), weathering of materials, and most of biological process [1]. One of the main interests of this reaction focused on its role in oxygen electrode used in electrical-power related systems, i.e. metal-air batteries and fuel cells. From this point of view, being an abundantly available transitional metal oxides, Nickel cobaltite,  $\text{NiCo}_2\text{O}_4$ , have immediately shows many advantages, compared to already available alternatives. In catalysis,  $\text{NiCo}_2\text{O}_4$  has a role as heterogenous catalyst with the reaction of ORR. However the mechanism of ORR on metal surfaces is still remains unclear.  $\text{NiCo}_2\text{O}_4$  indicates a half-metallic property, according to low field magnetoresistance (LFMR) measurements [2]. Nickel cobaltite is also reported to be half metallic with  $-19.1\%$  low-field magnetoresistance at 0.5 T and  $-50\%$  at 9 T (both measured at 2 K) [2]. Combined with its high Curie temperature (295K [3], 350K [4]), these properties made nickel cobaltite into good candidate as spintronic materials. One can easily tune its electrical and magnetic properties by varying the crystal growth temperature and oxygen pressure [5].

$\text{NiCo}_2\text{O}_4$  is a ferrimagnet [4, 6] and one candidate of novel materials that could be engineered in many ways to exhibit different properties. By utilizing temperature growth of less than  $450^\circ\text{C}$ , one can acquire metallic-ferrimagnetic  $\text{NiCo}_2\text{O}_4$  thin film. On the contrary, with more than  $450^\circ\text{C}$ , we would acquire thin film as non-magnetic insulator [7]. This uniqueness is believed to come from the competition between double exchange interaction among cations with different charges and superexchange interaction among those with same charges [3].

Electronic structure investigation from theoretical approach was reported in the work combined with the experimental measurement [8]. The authors have used a modified Becke-Jonson formula in the exchange-correlation function based on local spin density approximation (mBJ-LDA). It reported large energy gaps of around 3–4 eV in majority spin states between the valence and conduction bands, and the result indicated a half-metallic property. The properties of electronic structure, such as large energy gap, have not been validated yet and the details on electronic structure are not so clear that they are self-consistently understood with the properties of catalysis. The successive theoretical approach, namely LDA+U approach, introduced an on-site Coulomb parameter of Hubbard model,  $U_{\text{eff}}$ , to the cation sites [2, 5].

### 1.2 Research Objectives

Theoretical investigation on electronic and magnetic properties of bulk  $\text{NiCo}_2\text{O}_4$  is needed to understand its basic features. In this theoretical investigation, quasi-particle self-consistent GW (QSGW) calculations [9–11] were performed in normal and inverse spinels of  $\text{NiCo}_2\text{O}_4$ . This method does not employ any empirical parameter like  $U_{\text{eff}}$ . This feature indicated a lot of advancements in the electronic structure analyses of semi-conducting and insulating materials. The QSGW calculation enables to calculate metallic electronic structures. Such advantage may be useful for a wide range of materials in the advanced methods beyond the density functional theory (DFT) [12] approach. The performance of QSGW beyond DFT in improving the electronic structure of semiconductors has been well known already [10]. The recent progress has been reached to a group of materials for power electronics [13, 14] and a group of surfaces [15]. At the same time, we investigate the performance of QSGW method in analyzing half-metallic materials. The performance of QSGW method in predicting the energy band gap of semiconductor is already well known. We put a confirmation on this by calculating the properties of  $\text{Co}_3\text{O}_4$ .

## 2 COMPUTATIONAL METHOD

Spinel materials or their family are usually presented as a chemical formula  $\text{XY}_2\text{O}_4$ , where X and Y are cationic elements. For the cationic elements, there are two distinguishable atomic sites. They have tetrahedral and octahedral symmetries, being called tetrahedral and octahedral sites, respectively. There are 2

**Table 1:** Configurations of tetrahedral and octahedral sites for X and Y elements in spinel structure  $XY_2O_4$ . The numbers in parentheses are the number of atoms per formula unit.

system	octahedral site (4)	tetrahedral site (2)
Normal	Y(4)	X(2)
Inverse type A	X(1), Y(3)	X(1), Y(1)
Inverse type B	X(2), Y(2)	Y(2)

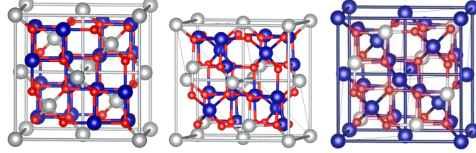


**Figure 1:** Three spinel structures of  $NiCo_2O_4$ . From left to right, they indicate spinels of normal, inverse type A, and inverse type B. Ni, Co, and O atoms are represented by silver, blue, and red color respectively.

tetrahedral sites and 4 octahedral sites in a primitive unit cell (two formula units). In the normal spinel, all of X occupies tetrahedral site and all of Y at octahedral site. In inverse spinel structure, X and Y atoms are interchanged with each other between the tetrahedral and octahedral sites. As in the previous work of  $NiCo_2O_4$  [7], we considered two types of inverse spinel, called Types A and B (inverse A and inverse B). The configurations of tetrahedral and octahedral sites for X and Y elements are presented in Table 1.

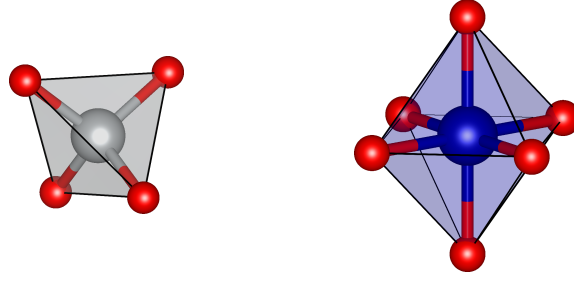
The crystal structure of normal spinel belongs to a face-centered cubic structure with the space group of No. 227. In case of  $NiCo_2O_4$ , its structure was reported to have an inverse spinel structure [6]. We calculated normal and two inverse spinel structures of  $NiCo_2O_4$ . The normal and inverse spinel structures (inverse A and inverse B) are presented in Figure 1. Silwal et.al. [7] suggested that the inverse B configuration has a higher tendency to happen rather than inverse A configuration. Our discussion in this paper, particularly focused on the inverse type B.

Figure 2 picks up atomic configurations at the tetrahedral and octahedral sites in spinel structure. Each cation atom is surrounded by four or eight oxygen atoms depending on these sites. Oxygen imposes a strong crystal field at the cation site. As a consequence of such crystal field, the five energy levels of 3d orbital will split into two kinds of levels denoted as  $t_{2g}$  (3 levels) and  $e_g$  (two levels). For the tetrahedral site surrounded by negatively charged oxygen, the  $t_{2g}$  levels are lowered and the  $e_g$  are raised. In octahedral site, this level arrangement is reversed. The energy width of this splitting may indicate degree of the crystal field.

We investigated optimized structure of lattice parameter  $a$  and internal parameter  $u$  using the house-package of DFT(GGA) code [16] for the normal spinel structure of  $NiCo_2O_4$ . As  $u$  increases, the oxygen tetrahedron around the cation of tetrahedral site expands, resulting in an elongation of cation-oxygen bond. They were determined to be  $a = 8.115 \text{ \AA}$  and  $u = 0.3881$ . The former was in agreement with the experimental values. Thus, we decided to use the set of experimental values in our further research. Indeed, we took the experimental values of  $a = 8.114 \text{ \AA}$  and  $u = 0.3833$  [6, 17]. The difference ( $\delta u$ ) between two internal parameters presented above corresponds to an oxygen atomic distortion of  $0.07 \text{ \AA}$  ( $=\sqrt{3}a \delta u$ ). This is much smaller than a standard bond length of Ni-oxide (0.4%) [6].

## 2.1 Hedin's Equation and QSGW Approximation

QSGW method is an approximation of GW method that based on a set of many body perturbation theory constructed by Hedin. In GW construction, we start from a Green's function of the system  $G$ . Using this initial Green's function, we should calculate polarization function  $\Pi$ . Furthermore, we calculate screened Coulomb function  $W$  to get a sigma function  $\Sigma$ . This particular  $\Sigma$  function will be used to get a



**Figure 2:** Atomic configurations of tetrahedral (left) and octahedral (right) sites, respectively. Silver or blue ball denotes a cation atom and red balls denote oxygen atom.

vertex function  $\Gamma$ . In the construction of GW method, these five functions created an iterative steps that theoretically would converged into ideal Green' s function of the system.

$$\begin{aligned}
\Sigma(1,2) &= i \int d(34)G(1,3^+)W(1,4)\Gamma(3,2,4) \\
G(1,2) &= G^0(1,2) + \int d(34)G^0(1,3)\Sigma(3,4)G(4,2) \\
\Pi(1,2) &= -i \int d3d4\Gamma(3,4,2)G(1,3)G(4,1^+) \\
W(1,2) &= v(1,2) + \int d(34)v(1,3)\Pi(3,4)W(4,2) \\
\Gamma(1,2,3) &= \delta(1-2)\delta(2-3) \\
&\quad + \int d(4567) \frac{\delta\Sigma(1,2)}{\delta G(4,5)} G(4,6)G(7,5)\Gamma(6,7,3)
\end{aligned}$$

In QSGW approach [11], we simplify the last equation for vertex function into  $\Gamma(1,2,3) = 1$  Initial  $G^0$  produced from DFT results:

$$\begin{aligned}
G^0 &= \sum_{nk} \frac{\psi_{nk}(r)\psi_{nk}^*(r')}{\omega - \epsilon_{nk} \pm i\eta} \\
V_{xc} &= \frac{1}{2} \sum_{n_1 n_2} |\psi_{n_1}\rangle \{Re[\Sigma^{GW}(\epsilon_{n_1})]_{n_1 n_2} + Re[\Sigma^{GW}(\epsilon_{n_2})]_{n_1 n_2}\} \langle\psi_{n_2}|
\end{aligned}$$

### 2.1.1 Convergence criteria

In usual self-consistent procedure, i.e. Hartree-Fock or Density Functional Theory, the convergence is usually based on the total energy of the system. By following the variational principle, we can iteratively change the wave function in such a way that it would produce the lowest total energy. This lowest total energy would corresponds to the final wave function of the ground state of our studied system. However, the calculation of total energy in GW construction is still under heavy development, theoretically. As a workaround, we performed a convergence check on eigen values of the wave function, spanning on calculated k-points. This raise a question on the convergence criteria, because each eigen values would dynamically changed in each iteration without any pattern that can be followed to deduce the next step of iteration. However, by concentrating our criteria on eigen values around Fermi level, and noticing that usually lowest energy bands would converge more rapidly than those from higher energy, we can conclude quite robust convergence criteria.

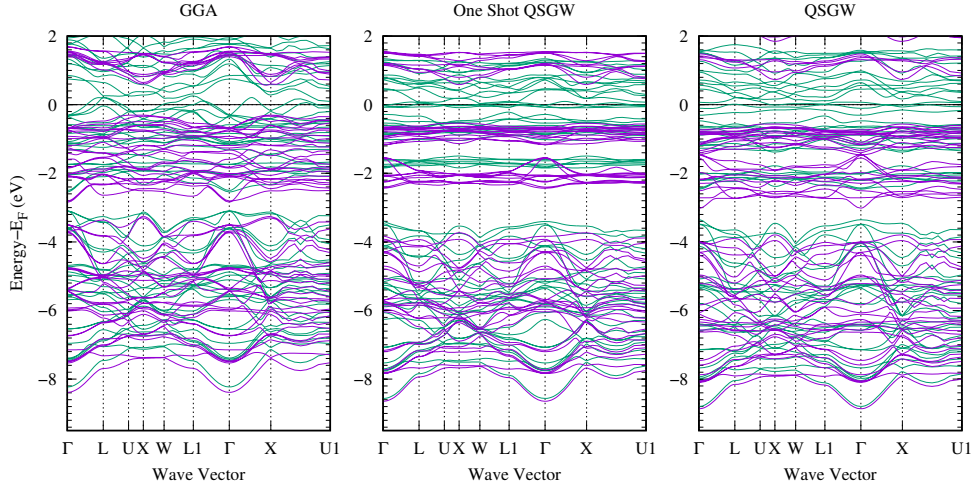


**Figure 3:** The energy band dispersions for  $\text{NiCo}_2\text{O}_4$  with the inverse spinel type-B structure, green indicates minority spin states and magenta for majority ones. From left to right, the results of GGA, one-shot QSGW, and QSGW. The Fermi level presented by horizontal line is set at zero energy.

### 3 RESULTS AND DISCUSSION

#### 3.1 $\text{NiCo}_2\text{O}_4$

##### 3.1.1 *Electronic structure*

As shown in Figures 3, the valence band around the Fermi level consists of the three parts of oxygen orbital and two cation 3d orbitals. As a whole property, the band width of cation bands becomes narrow from GGA to QSGW. These features are detailed in total and projected density of states (PDOS) obtained from GGA, one-shot GW, and QSGW that are shown in Figures 4. All of PDOS display metallic behaviour only at the minority spin state. The cation band around the Fermi level is distributed, as if supposing the crystal field of octahedral or tetrahedral site. In these GW results, the crystal field effect appears more clearly than those of GGA. This may be caused by the Coulomb interaction affected from O is taken into account more accurately through the screened Coulomb interaction  $W$ . The localization of electron wave functions and stabilization on oxygen band also identified from Figures 4.

The half-metallicity in the present work is in agreement with the previous theoretical results including the mBJ-LDA [8] and the LDA+U approaches [2, 5]. We note some features during the self-consistent iterative cycle by comparing the PDOS between one-shot GW and QSGW. First, the degree of energy splitting from crystal field increases in the self-consistent process. Second, as a result, the sharpness of DOS in one-shot GW becomes broaden, but have never reached to a broadness of DOS like GGA. Using GGA method, we found band gap at majority spin of 0.85 eV, 0.82 eV and 0.84 eV for normal spinel structure, inverse A-type structure, and inverse B-type structure, respectively. All structure type, shown that majority spin valence bands are dominated by octahedral sites 3d  $t_{2g}$  orbitals, with minor contribution from tetrahedral sites 3d  $t_{2g}$  orbitals. On the other hand, the conduction band is composed by 3d  $e_g$  orbitals of all atoms that occupy octahedral sites, i.e. all Co in normal spinel, Co and Ni atoms in inverse spinel structure. Our calculation shown that localized 3d states consistently appeared between range of -0.25 eV to -2.5 eV on octahedral sites, regardless atom element that occupy those sites. All structure exhibited delocalized O 2p orbitals below  $E_f$ . For minority spin, our calculation shown that DOS around  $E_f$  is dominated by atoms that occupied tetrahedral sites. However, in case of Ni(Td), we have 3d  $t_{2g}$  orbitals that fulfill this role, while in case of Co, we have 3d  $e_g$  orbitals.

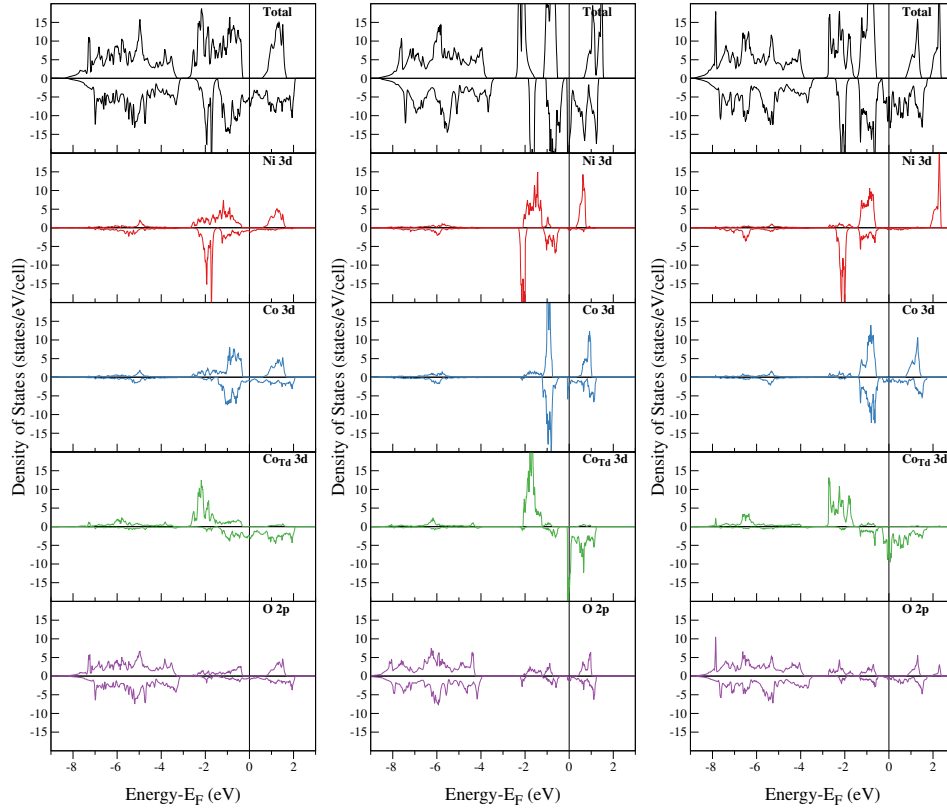


**Figure 4:** Total and projected densities of states (DOS) of the Ni(oct) 3d, Co(oct) 3d, Co(tet) 3d, and O 2p orbitals of inverse type B spinel  $\text{NiCo}_2\text{O}_4$  for GGA, one-shot GW, and QSGW.

### 3.1.2 Magnetic configuration

All of the methods (GGA, one-shot GW, and QSGW) provide a net magnetization of  $2 \mu_{\text{B}}/\text{f.u.}$  (f.u.: formula unit.) in the inverse spinel structures of type A and type B, and also normal spinel structure. This value of net magnetization has been reported in the previous works [4]. Both inverse structures provide a ferrimagnetic arrangement, whereas the normal spinel structure exhibits ferromagnetic arrangement. However, the ferrimagnetic arrangement provided by the inverse type A has a significant difference with that of type B. This is due to the difference of cation configuration between the inverse type A and type B.

Our total magnetization is much larger than the experimental value ( $1.25 \mu_{\text{B}}/\text{f.u.}$ ) [6]. Recent experiment [2] reported that the total magnetization gradually increases to a larger value ( $1.84 \mu_{\text{B}}/\text{f.u.}$ ) as the annealing time of specimen increases. This difference on the magnetization may be attributed to a disordered crystal structure in experimental specimen.

Magnetic moment on each atom varied from GGA to QSGW, as shown in Table 2. The ferrimagnetic configuration of inverse Type B is clearly indicated. The QSGW consistently shows a larger absolute value for each atomic magnetic moment except for Co(oct).

### 3.1.3 Electron configuration

The electron configuration of atom in solid crystal may not be the best way to represent using the ionic representation for cation elements. However, such a way is helpful to understand pictures of electronic state more deeply. As a speculation, the electron configuration at the atomic state may be presented as Co(Td) 3d  $(d\uparrow)^5(d\downarrow)^2$ , Ni 3d  $(d\uparrow)^{3.5}(d\downarrow)^5$ , and Co 3d  $(d\uparrow)^{3.5}(d\downarrow)^{3.5}$ .

### 3.1.4 Properties at the Fermi level

The electronic states near the Fermi level consist mainly of the 3d-orbitals on Ni(oct) and Co(oct) in the majority spin state, and of the 3d orbitals on Co(tet) in the minority spin state. In Table 3, the total

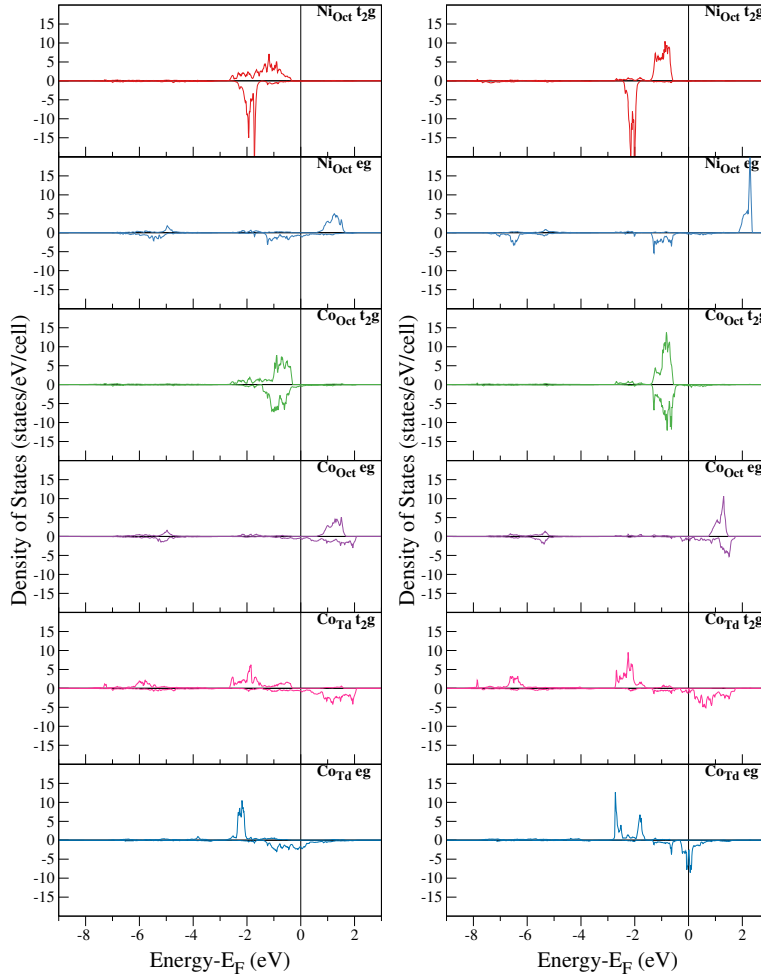


**Figure 5:**  $t_{2g}$  and  $e_g$  components for projected density of states on Ni 3d and Co 3d orbitals in inverse type B spinel of  $\text{NiCo}_2\text{O}_4$  from GGA and QSGW.

and partial DOS at the Fermi level (inverse type B) are reported for GGA and QSGW. The total DOS is similar to each other and the main contribution is from Co(tet). However, there are remarkable difference on its component. The components of Ni(tet), Co(oct), and O decreases from GGA to QSGW, whileas the component of Co(oct) increases. These changes implies a large change at electronic state of the Fermi level.

### 3.1.5 Comparison with $\text{NiCo}_2\text{S}_4$

Here, we have shown at Figure 6 energy gap around  $E_F$  (eV) for Inverse B  $\text{NiCo}_2\text{O}_4$  are 0.82 (GGA) and 1.15 (QSGW). This should be compared to experiment value of 2.58 eV. For  $\text{Co}_3\text{O}_4$  in Figure 6, we found that QSGW produced much larger energy gap of 2.88 eV, compared with 0.33 eV from GGA results. This energy gap is comparable with experiment value of 2.9 eV. QSGW systematically enlarge the pseudo-bandgap at majority spin. For  $\text{Co}_3\text{O}_4$ , we have an antiferromagnetic configuration with zero total magnetization. Here, QSGW shows its quality in predicting better band gap for semiconducting  $\text{Co}_3\text{O}_4$ .

Antiferromagnetic nature of  $\text{Co}_3\text{O}_4$  coming from 3d orbital of Co at both tetrahedral sites. Octahedral sites of  $\text{Co}_3\text{O}_4$  have zero contribution on magnetization. QSGW predicted that 3d orbital of Co at tetrahedral sites is fully occupied. This is in accordance to the tendency of QSGW for showing more localized electrons than GGA. On the other hand, Co(Oct) of  $\text{NiCo}_2\text{O}_4$  shows similiarly small contribution to magnetization. The main contribution to magnetization in  $\text{NiCo}_2\text{O}_4$  comes from both Co(Oct) and Ni(Td), with the later atoms have the highest contribution. However, conductivity of  $\text{NiCo}_2\text{O}_4$  is indicated to be mainly contributed by Co at tetrahedral sites. Crystal field of metals at A and B sites also visible.

The spin densities at Figure 7 were generated by taking the density difference between minority and majority spin at all space. From this density, we can see that in  $\text{NiCo}_2\text{O}_4$ , Co(Oct) have no contribution to

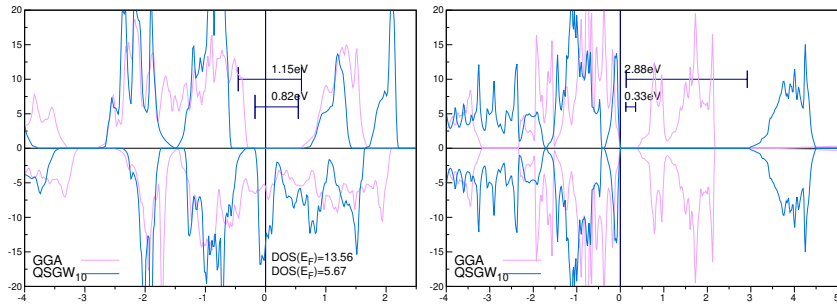


**Figure 6:** Total density of states of  $\text{NiCo}_2\text{O}_4$  and  $\text{Co}_3\text{O}_4$ , from left to right respectively.

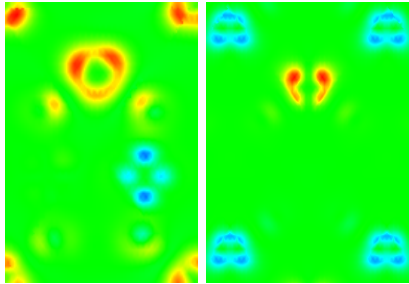


**Figure 7:** Spin density for  $\text{NiCo}_2\text{O}_4$  and  $\text{Co}_3\text{O}_4$  mapped on to 110A plane.

the magnetization, in agreement with the results of Partial Density of States. Furthermore, Ni atoms are in antiparallel with Co(Td). We also notice the strong  $d\epsilon$  orbital character shown by Ni. On the other hand, ferrimagnetic property of  $\text{Co}_3\text{O}_4$  comes from antiparallel spin between two tetrahedral sites.

## 4 CONCLUSIONS

We have performed first-principles investigation on electronic structure in the half-metallic inverse spinel nickel cobaltite  $\text{NiCo}_2\text{O}_4$  using a QSGW method. The GWA of QSGW was found to conduct the narrower band widths in the band mainly consisting of the cation 3d-orbitals, implying localized wave functions in the electronic structure. The energy level splitting of  $t_{2g}$  and  $e_g$  caused by its crystal field from the PDOS results is more clearly observed than those in the GGA case. The main contribution to the states at the Fermi level is found to be from Co(tet) 3d  $e_g$  orbitals. The possible states of Ni(oct)  $e_g$ , Co(oct)  $e_g$  and others are largely suppressed. As in the previous calculations, the electronic structure calculation from QSGW also confirms that the material  $\text{NiCo}_2\text{O}_4$  is a promising candidate for spintronics application due to its half-metallicity. We also confirm the performance of QSGW method in predicting electronic property of semiconducting  $\text{Co}_3\text{O}_4$ . Comparing  $\text{NiCo}_2\text{O}_4$  and  $\text{NiCo}_2\text{S}_4$ , we found that metallic behaviour mainly come from hybridization between 3d orbital of Co(Td) with p orbital of oxygen or sulfide. We also found that sulfide anion provides more localized electron than Oxygen anion. The introduction of Ni induces  $\text{NiCo}_2\text{O}_4$

**Table 2:** Atomic and total magnetic moments ( $\mu_B$ ) in  $\text{NiCo}_2\text{O}_4$  (inverse type B) from GGA, one-shot GW, and QSGW. Note that the averaged value is presented at O 2p.

Atom	GGA	one-shot GW	QSGW
Co(tet) 3d	2.34	2.77	2.77
Ni(oct) 3d	-0.87	-1.27	-1.39
Co(oct) 3d	0.09	0.02	0.07
O 2p	0.07	0.09	0.10
Sum in f.u.	1.81	1.86	1.86
Total in f.u.	2.00	2.00	2.00

**Table 3:** Total and projected DOS  $N_{\downarrow}$  at  $E_F$  (states/eV/cell) in inverse B from GGA and QSGW. At the row of "O 2p", all O 2p contributions are included and at the row of "Sum" the summation of atomic values are reported.

$N_{\downarrow}(E_F)$	GGA	QSGW
Co(tet) 3d	2.45	3.50
Ni (oct) 3d	0.92	0.16
Co (oct) 3d	0.82	0.42
O 2p	0.82	0.53
Sum	5.01	4.61
Total	5.67	6.15

to be metallic. However, at the end, Ni would have minimal contribution to the single-spin state conductivity (half-metal). Unfortunately, the present calculation fails to describe an insulating/semiconducting property inherent to the  $\text{NiCo}_2\text{O}_4$  at low temperatures. This new problem should be solved with a more accurate treatment in an advanced electronic structure calculation.

## REFERENCES

- [1] B Chi, H Lin, J Li, N Wang, J Yang, International Journal of Hydrogen Energy 2006, 31, 1210–1214.
- [2] P. Li, C. Xia, D. Zheng, P. Wang, C. Jin, H. Bai, physica status solidi (RRL) – Rapid Research Letters 2016, 10, 190–196.
- [3] Y. Bitla, Y.-Y. Chin, J.-C. Lin, C. N. Van, R. Liu, Y. Zhu, H.-J. Liu, Q. Zhan, H.-J. Lin, C.-T. Chen, Y.-H. Chu, Q. He, Scientific Reports 2015, 5, DOI [10.1038/srep15201](https://doi.org/10.1038/srep15201).
- [4] G Blasse, Philips Research Reports 1963, 18, 383.
- [5] K. Zhang, C. Zhen, W. Wei, W. Guo, G. Tang, L. Ma, D. Hou, X. Wu, RSC Advances 2017, 7, 36026–36033.
- [6] O. Knop, K. I. G. Reid, Sutarno, Y. Nakagawa, Canadian Journal of Chemistry 1968, 46, 3463–3476.
- [7] P. Silwal, L. Miao, I. Stern, X. Zhou, J. Hu, D. H. Kim, Applied Physics Letters 2012, 100, 032102.
- [8] K. Dileep, B. Loukya, P. Silwal, A. Gupta, R. Datta, Journal of Physics D: Applied Physics 2014, 47, 405001.
- [9] S. V. Faleev, M. van Schilfgaarde, T. Kotani, Physical Review Letters 2004, 93, Publisher: American Physical Society, 126406.
- [10] M. van Schilfgaarde, T. Kotani, S. Faleev, Physical Review Letters 2006, 96, Publisher: American Physical Society, 226402.
- [11] T. Kotani, M. van Schilfgaarde, S. V. Faleev, Physical Review B 2007, 76, 10.1103/PhysRevB.76.165106.
- [12] W. Kohn, L. J. Sham, Physical Review 1965, 140, A1133–A1138.
- [13] J. Otsuka, T. Kato, H. Sakakibara, T. Kotani, Japanese Journal of Applied Physics 2017, 56, Publisher: IOP Publishing, 021201.
- [14] A. Sawamura, J. Otsuka, T. Kato, T. Kotani, Journal of Applied Physics 2017, 121, Publisher: American Institute of Physics, 235704.
- [15] H. Sakakibara, T. Kotani, M. Obata, T. Oda, Physical Review B 2020, 101, Publisher: American Physical Society, 205120.
- [16] T. Oda, A. Hosokawa, Physical Review B 2005, 72, Publisher: American Physical Society, 224428.
- [17] M. G. Brik, A. Suchocki, A. Kamińska, Inorganic Chemistry 2014, 53, 5088–5099.

## 学位論文審査報告書（甲）

## 1. 学位論文題目（外国語の場合は和訳を付けること。）

Electronic structures of spinel nickel cobaltite from a spin-polarized quasi-particle self-consistent GW method (和訳：スピン分極準粒子自己無撞着 GW 法によるスピネル-ニッケル-コバルタイトの電子構造)

2. 論文提出者 (1) 所属 数物科学 専攻

(2) 氏名 Hasan Al Rasyid

## 3. 審査結果の要旨（600～650字）

学位論文について、各審査委員が個別に検討した後、令和2年7月22日に予備審査会を実施し、論文内容を詳細に検討した。その後、令和2年8月5日に実施された口頭発表後に審査委員会を開催し、協議の結果以下のように判定した。

Hasan Al Rasyid氏は、三元磁性化合物のスピネル-ニッケル-コバルタイト( $\text{NiCo}_2\text{O}_4$ )の電子構造を、スピン分極準粒子自己無撞着 GW(QSGW)法を用いて初めて解析した。ここでGWは、電子のグリーン関数  $G$  と遮蔽されたクーロン相互作用  $W$  の積により電子の自己エネルギーを計算する量子力学における近似を意味し、GW法では、準粒子エネルギーを高い物理精度で求めることができる。近年、QSGW法で多くの成功例が示されてきたが、3元化合物や磁性体、金属への応用例は計算量の問題があり、これまで研究が進んでいなかった。Hasan Al Rasyid氏は、触媒材料やスピントロニクス材料への応用が期待されるハーフメタリック酸化物  $\text{NiCo}_2\text{O}_4$  での電子構造解析を通して、密度汎関数法等の従来法に対するQSGW法の格段の優位性を明らかにした。多元金属磁性体系でのQSGW法の成功を示したことは、強相関電子系の物性科学、計算物質科学の進展に寄与するものである。以上により、本論文は博士(理学)の学位に値すると判定した。

4. 審査結果 (1) 判定 (いずれかに○印) 合格 ・ 不合格

(2) 授与学位 博士(理学)